Available online at www.sciencedirect.com
ScienceDirect
Trans. Nonferrous Met. Soc. China 27(2017) 2613−2621
Transactions of Nonferrous Metals Society of China
www.tnmsc.cn

Microstructure and mechanical properties of laser additive repaired Ti17 titanium alloy

Zhuang ZHAO[1,2], Jing CHEN[1,2], Qiang ZHANG[1,2], Hua TAN[1,2], Xin LIN[1,2], Wei-dong HUANG[1,2]

1. State Key Laboratory of Solidification Processing, Northwestern Polytechnical University, Xi'an 710072, China;
2. Key Laboratory of Metal High Performance Additive Manufacturing and Innovative Design, Ministry of Industry and Information Technology, Northwestern Polytechnical University, Xi'an 710072, China

Received 15 August 2016; accepted 27 February 2017

Abstract: Laser additive manufacturing technology with powder feeding was employed to repair wrought Ti17 titanium alloy with small surface defects. The microstructure, micro-hardness and room temperature tensile properties of laser additive repaired (LARed) specimen were investigated. The results show that, cellular substructures are observed in the laser deposited zone (LDZ), rather than the typical α laths morphology due to lack of enough subsequent thermal cycles. The cellular substructures lead to lower micro-hardness in the LDZ compared with the wrought substrate zone which consists of duplex microstructure. The tensile test results indicate that the tensile deformation process of the LARed specimen exhibits a characteristic of dramatic plastic strain heterogeneity and fracture in the laser repaired zone with a mixed dimple and cleavage mode. The tensile strength of the LARed specimen is slightly higher than that of the wrought specimen and the elongation of 11.7% is lower.

Key words: laser additive repair; Ti17 titanium alloy; microstructure; mechanical properties; deformation behavior

1 Introduction

Ti17 (Ti−5Al−2Sn−2Zr−4Mo−4Cr) is classified as "β-rich" $\alpha+\beta$ titanium alloy, developed by GE in 1970s. It is widely employed to fabricate gas turbine engine components, such as disks for fan and compressor stages due to its excellent comprehensive service performances [1,2]. However, due to their severe service environment, it also means that these components are easy to be damaged, resulting in a material waste and overtime costs.

In order to reverse huge losses both on economy and delivery time resulted from damage, recently, based on the laser additive manufacturing (LAM) process with powder feeding, laser additive repair (LAR) technology has been developed [3,4]. Since LAM can be employed to fabricate fully dense and three dimensional components with high performance and complex structure, if we set the damaged components as the substrate, and build up worn sections of the metal components, the geometrical properties and mechanical properties of the damaged components could be restored. Compared with the conventional repair technologies, such as thermal spraying, welding, and brushing electro-plating, LAR has the advantages of excellent flexibility, controllable heat input introduced into the damaged components, and reasonable repairing cost [5,6]. It has been gradually applied to repairing the damaged components especially for the valuable structural titanium alloys.

Since the LAR technique shows a great potential for repairing damage structural components, the microstructures and mechanical properties of the final parts are common concerns of the recently studies. It is well documented that typical columnar β grains grow epitaxially from the substrate in the laser deposited zone. The α phase precipitates within the prior β grains during cooling [7,8]. Researches on the LAMed Ti17 titanium alloy have revealed that the microstructure characterization is quite sensitive to the thermal conditions, resulting in complex α phase morphology in the LAM process, such as superfine basket-wave microstructure, lamellar structure and layer bands [9−11]. There is no

Foundation item: Project (2016YFB11000100) supported by the National Key Technologies R&D Program, China; Project (KP201611) supported by Research Fund of the State Key Laboratory of Solidification Processing (NWPU), China; Project (51475380) supported by the National Natural Science Foundation of China
Corresponding author: Jing CHEN; Tel: +86-29-88460801; Fax: +86-29-88495106; E-mail: phd2003cjj@nwpu.edu.cn
DOI: 10.1016/S1003-6326(17)60289-9

surprising that variety of microstructure characterizations in the laser deposited zone (LDZ) would give different mechanical properties for LARed specimen. XUE et al [12] reported that the laser deposited zone and the wrought substrate could be treated as a combination of “strong + weak” for Ti64 titanium alloy, due to the superfine basket-wave microstructure formed in the laser deposited zone. LIANG et al [10] investigated the microstructure and mechanical behavior of Ti/Ti−6Al−2Zr−1Mo−1V structurally graded material (SGM) fabricated by LAM and figured out that the SGM specimen exhibited higher tensile strength and scattered premature necking behavior compared with CP-Ti specimens. RICHTER et al [13] evaluated the tensile properties of the LARed Ti6242 titanium alloy, and suggested that the testpieces exhibited slightly higher strength and significantly poorer plastic elongation compared with wrought specimens. ZHU et al [14] reported the fracture of the LAR Ti−6.5Al−3.5Mo−1.5Zr−0.3Si titanium alloy occurred in the wrought substrate zone during tensile testing, which meant that the laser deposited zone and bonding zone had better tensile strength than the substrate zone.

However, most of previous reports focused on the microstructure and mechanical properties of the LARed specimens with large laser deposited zone ratio (the volume fraction of the laser deposited zone on the tensile gauge part), such as 50% LARed specimen, i.e. the volume fraction of LDZ set as 50%. Table 1 provides a summary of the LDZ ratio, alloys studied and the corresponding repaired types extracted from the previous reports. It can be seen that a wide range of LDZ ratio from 20% to 60% has been investigated. Considering common mis-machining damage occurred during the productive process or foreign object damage encountered in service, the defect ratio may be very small, such as surface defect or hole-defect. Therefore, it is necessary to investigate the microstructure and mechanical properties of LARed Ti17 titanium alloy with small LDZ ratio, set as 0.5% in this study.

Table 1 Summary of laser deposited zone ratio reported in literature and reviewed in this study

Alloy system	LDZ ratio/%	Repaired type	Ref.
0Cr17Ni4Cu4Nb	30, 60	Surface repair	[5]
Ti−6Al−4V	25, 50	Surface repair	[12]
Ti−6242	50	Body repair	[13]
Ti−6.5Al−3.5Mo−1.5Zr−0.3Si	50	Body repair	[14]
IN718	50	Body repair	[15]
IN718	50	Body repair	[16]
Ti17	50	Body repair	[17]
1Cr12Ni2WMoVNb	50	Body repair	[18]
Ti−6Al−4V	20	Groove repair	[19]
Ti−6Al−4V	45	Surface repair	[20]
Ti17	0.5	Surface repair	This study

In order to obtain a deep understanding of the LARed Ti17 titanium alloy with small LDZ ratio, the microstructure, micro-hardness and room temperature tensile behaviors of LARed specimen were investigated systematically in this work. The microstructure evolution in the laser deposited zone during LARed process was further discussed.

2 Experimental

Considering the common surface defects on the loading structural components, typical hole-defect with 2 mm in diameter and 0.5 mm in depth (0.5% LDZ ratio) was prefabricated on the plate tensile specimen of forged Ti17 titanium alloy. The sketch is shown in Fig. 1. The LAR process was carried out on a LAM system typed LSF-IV, established by State Key Laboratory of Solidification Processing, Northwestern Polytechnical University, which consisted of a 300W pulsed YAG laser, a five-axis numerical control working table, a powder feeder with a coaxial nozzle and a chamber filled with pure argon gas with the oxygen content less than 50×10^{-6}. The Ti17 powders with the diameter of 80−120 μm prepared by plasma rotating electrode were employed as the cladding materials. The chemical composition of the substrate and the powder alloy are listed in Table 2. Before the LAR experiment, the powders were dried in a vacuum oven at (120±10) °C for 2 h, the surfaces to be repaired were polished by abrasive papers and cleaned by sonication in acetone. Then, the LAR technology with mutually perpendicular scanning path was employed to accomplish the LARed specimens with the processing parameters listed in Table 3. The newly LARed specimens were tempered in a vacuum oven at 540 °C for 1 h to eliminate the residual stress.

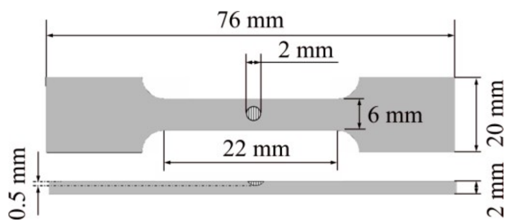

Fig. 1 Sketch of LARed specimen with prefabricated defect

Metallographic specimens were prepared using standard metallurgical procedures. A mixture solution of $HF+HNO_3+H_2O$ with a volume ratio of 1:3:50 was used as etching agent. The microstructures of the LARed Ti17

Table 2 Chemical compositions of Ti17 titanium alloy (mass fraction, %)

Alloy	Al	Sn	Zr	Mo	Cr	Fe	Si	N	H	O	Ti
Powder	5.18	2.15	2.06	4.06	4.05	0.017	0.026	0.012	0.004	0.089	Bal.
Substrate	5.15	2.14	2.08	3.98	4.10	0.011	0.033	0.012	0.004	0.087	Bal.

Table 3 Processing parameters of LARed Ti17 titanium alloy

Pulse width/ms	Laser scanning speed/(mm·s^{-1})	Percentage of laser power/%	Current/A	Frequency/Hz	Spot size of laser/mm	Powder feeder rate/(g·min^{-1})	Overlap/%
6−8	2	50	70−80	14	0.8	2−3	40−50

titanium alloy were characterized by optical microscopy and scanning electron microscopy. The phase constitution was analyzed by the X-ray diffraction (XRD) technique. Micro-hardness of the LARed specimen from WSZ to LDZ was measured by using Duranmin-A300 Vikers tester with 500 g load and 15 s dwelling time.

Tensile testing was performed at room temperature on an Instron−3382 testing machine with a constant crosshead displacement rate of 1mm/min. During tensile testing, strain evolution of the specimen was captured at a speed of 10 frames per second by 3D-DIC. This system used two high-speed cameras to collect real-timely speckle images. Speckles were prepared by matte painting sprayed on the surface of specimen before the test. Then, the digital speckle correlation method, computer binocular vision theory and mechanics theory of materials were introduced to trace the motion of specimen surface geometric points dynamically by analyzing the speckle images of the specimen surface before and after deformation. According to the motion of geometric points on the foundations of getting the 3D displacement filed, the 3D strain field could be calculated [21]. The wrought specimens were also tested under the same condition in order to compare with the LARed specimens. Three specimens of each coupon were tested for an average. The tensile fracture surface was examined using TESCAN VEGA II LMH scanning electron microscope.

3 Results and discussion

3.1 Microstructure characterization

The macrostructure of the LARed Ti17 titanium alloy is shown in Fig. 2. In terms of different microstructural characteristics, the LARed specimen can be divided into three zones: the laser deposited zone (LDZ), the heat affected zone (HAZ), and the wrought substrate zone (WSZ). As the first layer being deposited, the wrought substrate would be remelted. The remelting depth is generally small, and under conditions of the experiment the depth is about 50 μm. The wrought substrate which did not remelt near the side of LDZ underwent a reheat cycle during the LAR process, resulting in the changes in the regional microstructure and forming the HAZ. The depth of HAZ is about 150 μm. The substrate away from the LDZ keeps the original microstructure, which is the WSZ.

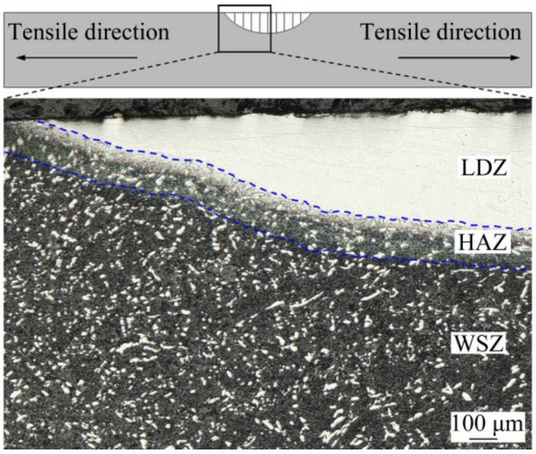

Fig. 2 Macrostructure of LARed Ti17 titanium alloy

Microstructures of the WSZ, HAZ and LDZ are shown in Figs. 3(a)−(d) respectively. In WSZ, typical duplex microstructure is observed with the equiaxial primary α and superfine β transformed microstructure (needle-like secondary α and retained β). The average size of equiaxial α is approximately 8 μm and the volume fraction of α phase is about 54% (Fig. 3(a)). This microstructure can be obtained easily by forging in the α+β phase field with a subsequent relatively slow cooling rate. As for the HAZ, the microstructure is almost identical with that of the WSZ except for some coarser secondary α and partly dissolved primary α from the WSZ to the LDZ, as shown in Fig. 3(b). In HAZ, an important character should be mentioned here is that no recrystallisation or grain growth is found. This is significantly different from the microstructures observed by the laser welded or large dimensional LARed titanium alloy [14].

Further observation of the microstructure in the LDZ is shown in Figs. 3(c) and (d). As indicated in Fig. 3(c), the significant fusion line, actually a region of planar growth, can be observed at the bottom of the

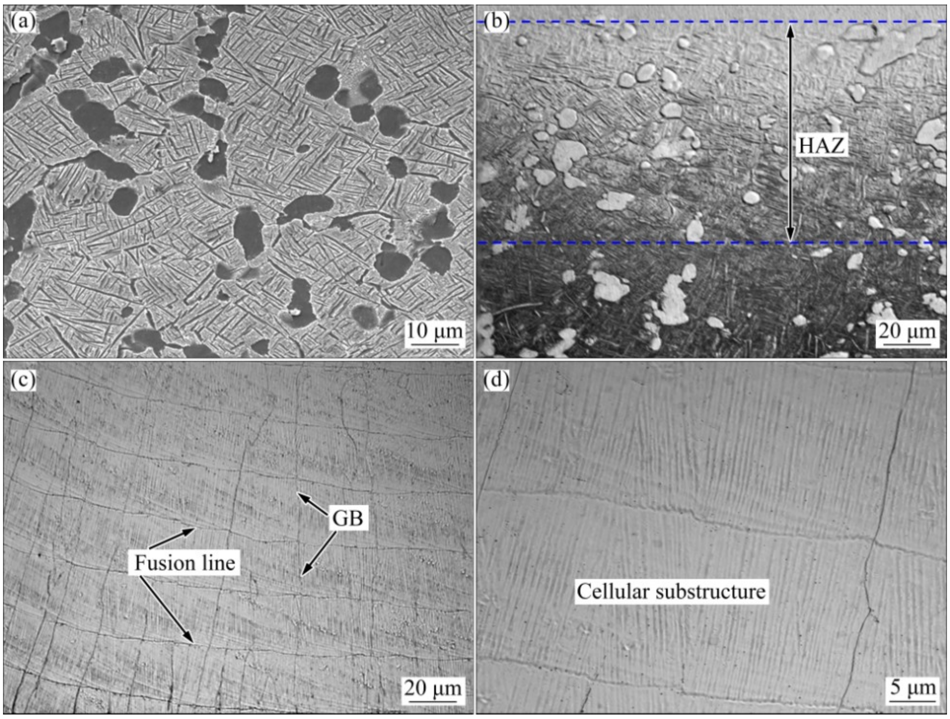

Fig. 3 Microstructures of LARed Ti17 titanium alloy: (a) WSZ; (b) HAZ; (c) LDZ; (d) Cellular substructure in LDZ

every cladding layers. Moreover, the columnar prior β grains extend consecutively through multiple layers due to the extreme solidification conditions in the LAR process (i.e. high thermal gradient and rapid solidification rate in the small melt pool). The width of the β grains is 20−50 μm. But, it is interesting to note that, no α phases precipitate on the prior β grain boundaries (GB). Moreover, as shown in Fig. 3(d), the cellular substructure can be observed clearly in the prior β grain. With the aid of XRD analysis, compared with the WSZ, no α peak in the LDZ has been found, as shown in Fig. 4. It indicates that the microstructure of the LDZ is single β phase. This is completely different from common microstructure in the laser additive manufactured titanium alloys, which usually consist of superfine basket-wave microstructure within the epitaxial columnar grains [22,23].

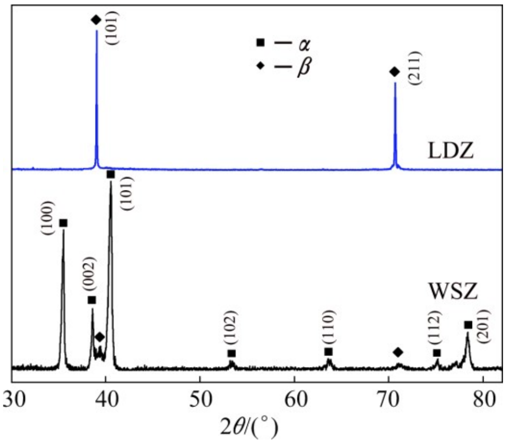

Fig. 4 XRD patterns of laser deposited zone and wrought substrate zone

3.2 Microhardness profile

Figure 5 shows the microhardness distribution on the cross-section of the LARed Ti17 titanium alloy. The microhardness of the LDZ is about HV 50 lower than that of the WSZ. Since the HAZ width is very narrow, the micro-hardness gradient in the HAZ is rather large, which sharply drops from HV 438 to HV 388. The microhardness distribution can be explained substantially by the microstructures as mentioned above. The WSZ is composed of equiaxial α and superfine β transformed microstructure, while the LDZ fills with cellular substructure instead of α phase or other β transformed

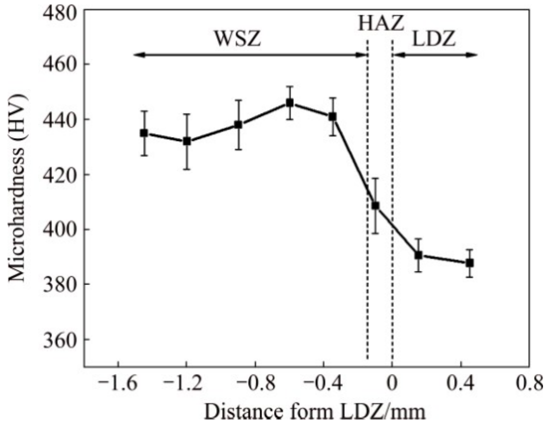

Fig. 5 Microhardness profile of LARed Ti17 titanium alloy specimen

microstructure in the prior β grains. This implies that, the α−β interfaces can hinder the dislocation slip in the WSZ and result in a higher microhardness. As for the HAZ, the superfine β transformed microstructures coarsen and primary α dissolves gradually from WSZ to LDZ. As a consequence, the α−β interface reduces gradually in the HAZ, resulting in a decline in the microhardness.

3.3 Room temperature tensile properties

Figure 6 shows the room temperature tensile properties of the LARed specimens and wrought specimens. It can be found that, both the yield strength ($\sigma_{0.2}$, 0.2% offset method) and ultimate strength (σ_b) of the LARed specimen are superior to those of the wrought specimen, while the tensile elongation of 11.7% is lower. As depicted in Fig. 7, the LARed specimens fracture in the repaired zone, which indicates that the laser repaired zone can be treated as a “weaker” region compared with wrought zone. Figure 8 shows the fracture surface of wrought specimen and LARed specimen. It can be found that both of the tensile fracture surfaces consist of fibrous zone (the blue region of the envelope) and shear rupture zone, but no obvious area reduction exists on the fracture surface of the LARed specimen. Moreover, the LDZ of the LARed specimen locates in shear rupture zone of the fracture surface, which implies that the crack initiation is also formed in the WSZ during tensile process. Magnification images of the fibrous zone surface of the two kinds of specimens are further examined by SEM, as shown in Figs. 8(a)−(b). On the fracture surfaces of wrought specimen, numerous dimples can be found, indicating that the wrought specimen is subjected to large plastic deformation prior to failure. Hence, the failure of wrought specimen is due to ductile fracture. The fracture surface of LARed specimen exhibits a feature of mixed dimple and cleavage mode as shown in Fig. 8(b), indicating the lower ductility of the LARed specimen.

Figure 9 illustrates the evolution of nominal stress−strain curve and the typical strain sequence of the

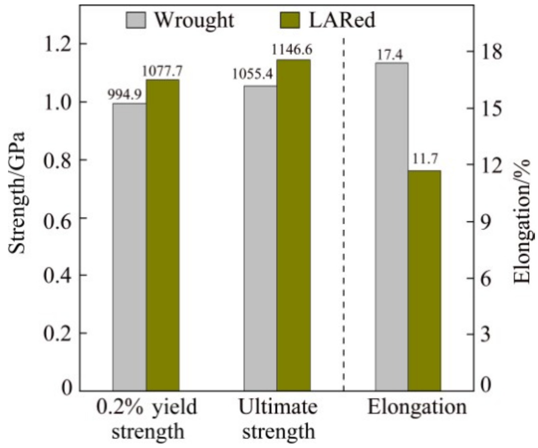

Fig. 6 Room temperature tensile properties of wrought specimen and LARed specimen

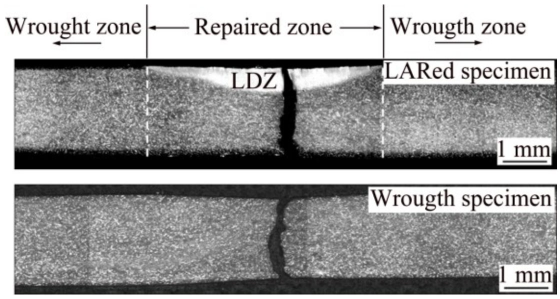

Fig. 7 View of tensile fracture of LARed and wrought specimens

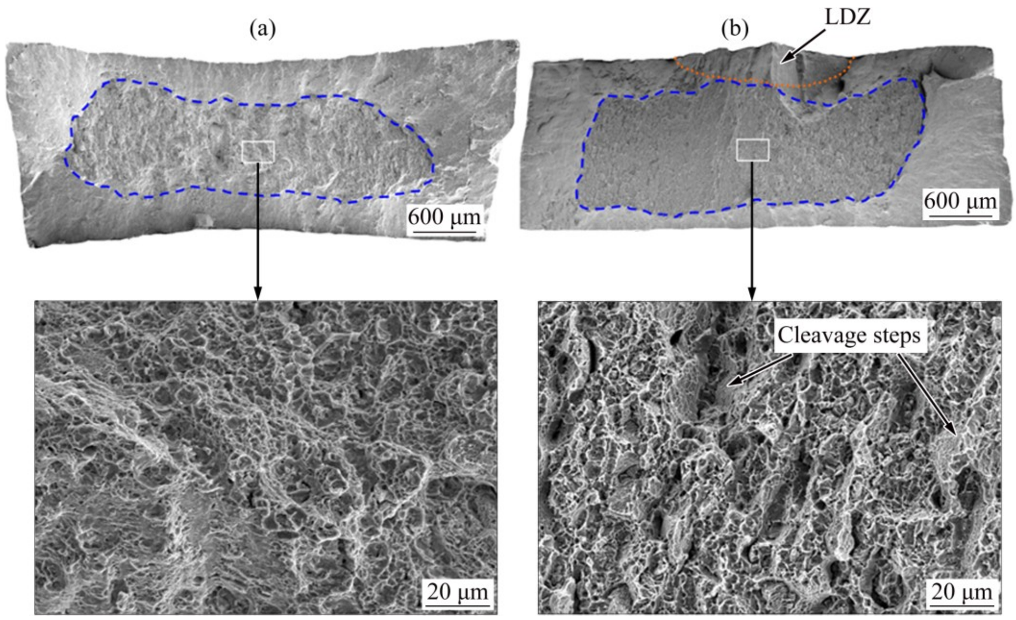

Fig. 8 Tensile fracture surface morphologies of Ti17 titanium alloy: (a) Wrought specimen; (b) LARed specimen

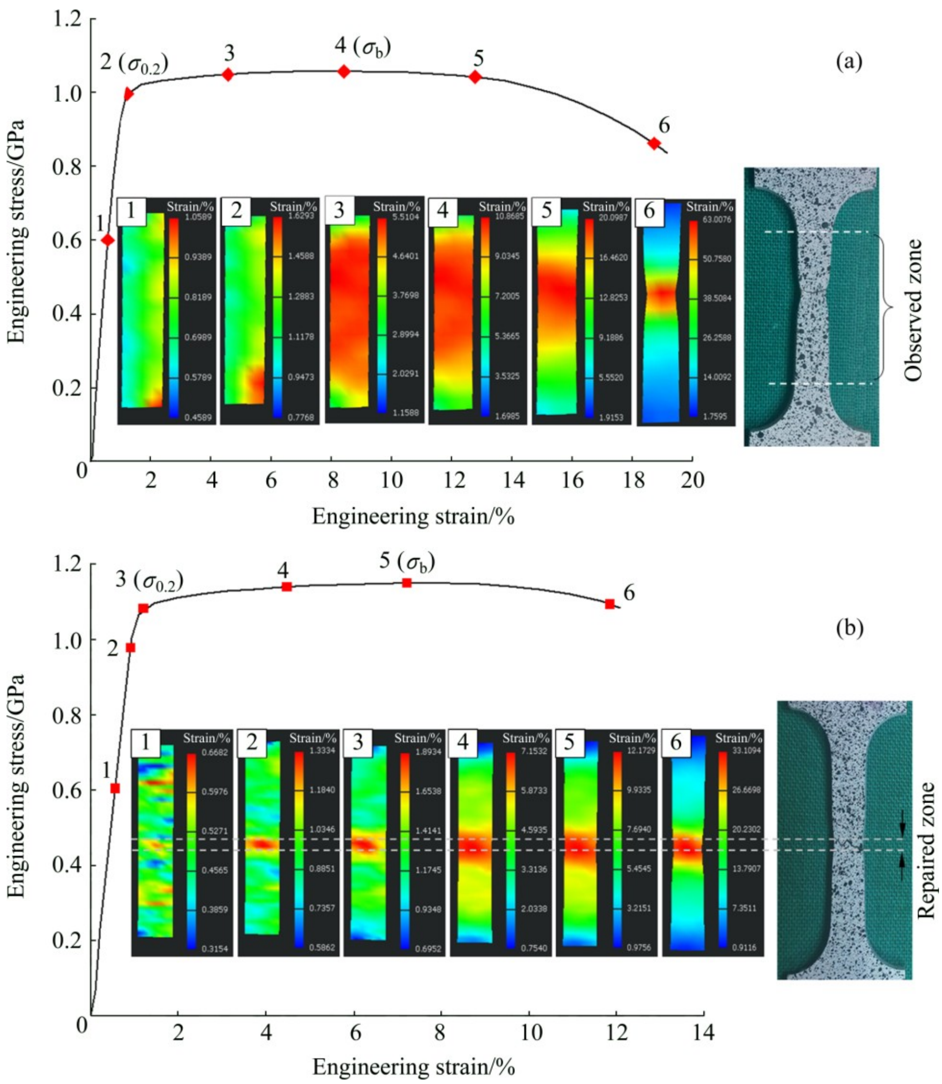

Fig. 9 Strain images sequence of Ti17 titanium alloy during tensile process: (a) Wrought specimen; (b) LARed specimen

wrought specimen and LARed specimen within the gauge length which is real-timely observed by DIC during tensile tests. And the color distribution in Fig. 9 reveals the tensile strain evolution in the specimen. From the results, it can be seen that the tensile strain distribution during the elastic stage of deformation is irregular for these two kinds of specimens. This implies that elastic deformation is almost uniform spread in the tensile gauge length. When the loaded specimen is stressed in some area above its yield limit, plastic deformation occurs and the distributions of tensile strains in the two kinds of specimen are quite different. It seems that strongly localized plastic strain firstly occurs in the LARed specimen and tensile maximum-strain is always concentrated in the repaired zone after yielding, due to the characteristic of structural heterogeneity and low strength-index produced in the LDZ. While the wrought specimen with uniform structure and mechanical properties takes the longest time for the appearance of strongly localized tensile strain until necking. During the deformation of strengthening stage, the maximum-strain of the wrought specimen can spread to the whole tensile gauge length from the initial yield position.

In general, in contrast to the wrought specimens, the LARed specimens exhibit a characteristic of dramatic plastic strain heterogeneity due to heterogeneous microstructure in the repaired zone. This plastic deformation behavior can significantly affect stress state of the repaired zone and the three-dimensional stresses can develop in this region. A similar phenomenon has been reported in the welded specimen with dramatic difference in mechanical properties [24,25]. According to the von Mises yielding criteria, the development of three-dimensional stresses will affect the yielding behavior of the materials. The yielding behavior is given by [26]

$$\sqrt{\frac{1}{2}\left[\left(\sigma_1-\sigma_2\right)^2+\left(\sigma_2-\sigma_3\right)^2+\left(\sigma_3-\sigma_1\right)^2\right]}\geq\sigma_\mathrm{s} \tag{1}$$

where σ_1, σ_2 and σ_3 are the three principal stresses respectively, σ_s is the purely axial tensile yield stress. Therefore, the LARed specimen might start to yield at a higher applied stress than that measured in the homogenous pure wrought specimen. Furthermore, this stress state can constrain the plastic deformation and advantage to cleavage fracture in the repaired zone. This is why the yield strength of the LARed specimen is slightly higher than that of wrought specimen and the LARed specimen exhibits inferior total elongation, as shown in Fig. 6.

3.4 Discussion

From the above results, the microstructure of the LDZ has significant difference from the microstructures obtained by the laser welded or large dimensional LAMed titanium alloy, which usually consists of superfine basket-wave microstructure within the epitaxial columnar grains. It is well document that the heat flow is extracted from the liquid melt pool to the wrought substrate or the previous consolidated layers during LAR process. The temperature gradient (G) and solidification velocity (v) play an important role in determining the solidification microstructure of the solid−liquid interface. For LAM, the G increases gradually from the top to the bottom of the molten pool and v is opposite [27]. So, it favors planar solidification at the bottom of each cladding layer. Moreover, for the Ti17, a β-metastable titanium alloy, the solute redistribution at the solid−liquid interface is remarkable. So, the liquid metal becomes undercooled, which is known as constitutional undercooling [28], and leads to the destabilization of the solidification front. When the temperature gradient at the solidification front decreases to a critical value, the solidification microstructure will be transformed from the planar growth to the cellular mode after a short distance away from the bottom of the molten pool, as shown in Fig. 3(d).

For the LAMed titanium alloys, typical α phase or other β transformed microstructure precipitated in the β matrix are a common phenomenon [7,9,10]. Formation of the α phase is contributed to the solid-state phase transformation. As we know, phase transformation path is determined by the cooling velocity [14,27]. The transformation process is schematically illustrated in Fig. 10 (dotted line represents the interrupted LAM process and subsequent continuous cooling). When cooling down from liquid phase (L), the L phase can transform to BCC β phase. Due to the fast cooling during the LAR process and high β stabilizers for Ti17 titanium alloy, the β phase transforms to the α phase or other β transformed microstructure will be completely suppressed in the first layer and the single β phase with typical solidification microstructure retained, as shown by v'_1 in Fig. 10. But, it is worth to note that the LAR process is a course of layer by layer deposition. It is equivalent to anneal the former layers as the current layer being deposited. Multiple reheating with a duration and amplitude will homogenize the solidification micro-segregation and lead to the formation of α phase or other β transformed microstructure in the former layers, as shown by v'_{N+1} in Fig. 10. This was consistence with the previous researches [29], in which the fully β microstructure was obtained in the top of a few deposited layers and the fine basket-wave microstructure was observed in the bottom of the LAMed Ti17 titanium alloy specimen.

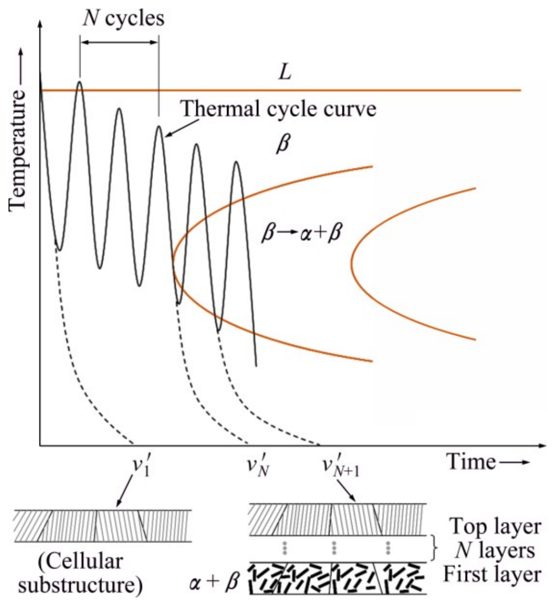

Fig. 10 Schematic illustration of microstructure formation mechanism in LDZ during LAR process

In this experimental condition, in contrast to large dimensional LAMed or high energy laser welded Ti17 titanium alloy, the scale of LDZ is much small with the LDZ ratio of only 0.5% and the laser energy input is lower in order to avoid thermal deformation in the damage substrate. This results in an inapparent thermal accumulation effect and fast cooling velocity in the former deposited layers due to lack of the enough subsequent thermal cycles. At low temperatures and short transformation time, the driving force is not large enough to enable nucleation and growth of the intracrystalline α phase. Therefore, the single β phase with typical solidification microstructure will be obtained in the LDZ.

In general, the microstructure characterization of the LAMed Ti17 titanium alloy is quite sensitive to the thermal conditions, which further depends on the process parameters and build dimension of the part being fabricated. Most of studies focus on the influence of process parameters on the microstructure. But, even though the same process parameters are used to fabricate Ti17 titanium alloy component with different LDZ ratios, which may also lead to different microstructure characterization and mechanical properties due to the different thermal histories experienced. Hence, in order to comprehensively understand the microstructure evolution, both the process parameters and LDZ ratio should be taken into consideration in the future.

4 Conclusions

1) The LARed Ti17 specimen with 0.5% LDZ ratio consists of three typical zones: laser deposited zone, heat affected zone and wrought substrate zone. In the LDZ, cellular substructure and single β phase are obtained in the prior β grains due to lack of the enough subsequent thermal cycles, which further results in a lower micro-hardness.

2) The tensile fracture of the LARed specimen occurs in the laser repaired zone with a mixed dimple and cleavage mode. The $\sigma_{0.2}$ and σ_b of the LARed specimen are 1077.7 MPa and 1146.6 MPa, respectively, which are slightly higher than those of wrought specimen. But the elongation of 11.7% of LARed specimen is lower than that of wrought specimen.

3) The LARed specimen exhibits a characteristic of dramatic plastic strain heterogeneity after yielding. This deformation feature significantly affects the yielding behavior of the LARed specimen and further leads to a higher tensile strength.

References

[1] LUO Jiao, LI Lian, LI Miao-quan. Deformation behavior of Ti−5Al−2Sn−2Zr−4Mo−4Cr alloy with two initial microstructure during hot working [J]. Transactions of Nonferrous Metals Society of China, 2016, 26(2): 414−422.

[2] ZHANG Qiang, CHEN Jing, TAN Hua. Microstructure evolution and mechanical properties of laser additive manufactured Ti−5Al−2Sn−2Zr−4Mo−4Cr alloy [J]. Transactions of Nonferrous Metals Society of China, 2016, 26(8): 2058−2066.

[3] QIAN Ting-ting, LIU Dong, TIAN Xiang-jun. Microstructure of TA2/TA15 graded structural material by laser additive manufacturing process [J]. Transactions of Nonferrous Metals Society of China, 2014, 24(9): 2729−2736.

[4] REN Hai-shui, TIAN Xiang-jun, LIU Dong. Microstructural evolution and mechanical properties of laser melting deposited Ti−6.5Al−3.5Mo−1.5Zr−0.3Si titanium alloy [J]. Transactions of Nonferrous Metals Society of China, 2015, 25(6): 1856−1864.

[5] LIN Xin, CAO Yong-qing, WU Xiao-yu. Microstructure and mechanical properties of laser forming repaired 17-4PH stainless steel [J]. Materials Science and Engineering A, 2012, (553): 80−88.

[6] GRUM J, SLABE J M. A comparison of tool-repair methods using CO2 laser surfacing and arc surfacing [J]. Applied Surface Science, 2003, 208−209: 424−431.

[7] CHEN Jing, ZHANG Feng-ying, LIN Xin. Laser repaid forming of low cost hydride-dehydride titanium alloy powder [J]. Transactions of Nonferrous Metals Society of China, 2006, 16(S): s2104−s2108.

[8] LI Zhen, TIAN Xiang-jun, WANG Hua-ming. Low cycle fatigue behavior of laser melting deposited TC18 titanium alloy [J]. Transactions of Nonferrous Metals Society of China, 2013, 23(9): 2591−2597.

[9] LORE T, FREDERIK V, TOM C. A study of the microstructure evolution during laser melting of Ti−6Al−4V [J]. Acta Materialia, 2010, (58): 3303−3312.

[10] LIANG Yao-jian, LIU Dong, WANG Hua-ming. Microstructure and mechanical behavior of commercial purity Ti/Ti−6Al−2Zr−1Mo−1V structurally graded material fabricated by laser additive manufacturing [J]. Scripta Materialia, 2014, 74: 80−83.

[11] SALIB M, TEIXEIRA J, GERMAIN L. Influence of transformation temperature on microtexture formation associated with α precipitation at β grain boundaries in a β metastable titanium alloy [J]. Acta Materialia, 2013, 61: 3758−3768.

[12] XUE Lei, CHEN Jing, LIN Xin. Microstructure and mechanical properties of laser rapid repaired Ti−6Al−4V Alloy [J]. Rare Metal Materials and Engineering, 2007, 36(3): 989−993.

[13] RICHTER K H, SVEN O, STEFFEN N. Laser cladding of the titanium alloy Ti6242 to restore damaged blades [C]//Proceeding of the 23rd International Congress on Applications of Lasers and Electro-Optics, Germany: Fraunhofer Institute, 2004.

[14] ZHU Yan-yan, LI Jia, WANG Hua-ming. Microstructure and mechanical properties of hybrid fabricated Ti−6.5Al−3.5Mo−1.5Zr−0.3Si titanium alloy by laser additive manufacturing [J]. Materials Science and Engineering A, 2014, 607: 427−434.

[15] BLACKWELL P L. The mechanical and microstructural characteristics of laser-deposited IN 718 [J]. Journal of Materials Processing Technology, 2005, 170: 240−246.

[16] QI H, AZER M, RITTER A. Studies of standard heat treatment effects on microstructure and mechanical properties of laser net shape manufactured INCONEL 718 [J]. Metallurgical and Materials Transactions A, 2009, 40: 2410−2422.

[17] CHEN Jing, ZHANG Qiang, LIU Yan-hong. Research on microstructure and high-temperature properties Ti17 titanium alloy fabricated by laser solid forming [J]. Chinese Journal of Lasers, 2011, 38: 0603022-1−7.

[18] WANG Yu-dai, TANG Hai-bo, FANG Yan-li. Microstructure and mechanical properties of hybrid fabricated 1Cr12Ni2WMoVNb steel by laser melting deposition [J]. Chinese Journal of Aeronautics, 2013, 26: 481−486.

[19] BENJAMIN G, ANDREY G, MICHAEL R. Laser metal deposition as repair technology for stainless steel and titanium alloys [J]. Physics Procedia, 2012, 39: 376−381.

[20] PAYDAS H, MERTENS A, CARRUS R. Laser cladding as repair technology for Ti−6Al−4V alloy: Influence of building strategy on microstructure and hardness [J]. Materials and Design, 2015, 85: 497−510.

[21] ZHU Fei-peng, BAI Peng-xiang, ZHANG Jing-bin. Measurement of true stress−strain curves and evolution of plastic zone of low carbon steel under uniaxial tension using digital image correlation [J]. Optics and Lasers in Engineering, 2015, 65: 81−88.

[22] WANG T, ZHU Y Y, ZHANG S Q. Grain morphology evolution behavior of titanium alloy components during laser melting deposition additive manufacturing [J]. Journal of Alloys and Compounds, 2015, 632: 505−513.

[23] STERLING A J, TORRIES B, SHAMSAEI N. Fatigue behavior and failure mechanisms of direct laser deposited Ti−6Al−4V [J]. Materials Science and Engineering A, 2016, 655: 100−112.

[24] ACAR M O, GUNGOR S. Experimental and numerical study of strength mismatch in cross-weld tensile testing [J]. Journal of Strain Analysis, 2015, 50: 349−365.

[25] ZHAO Shu-sen, YU Guang, HU Yao-wu. Microstructural and mechanical characteristics of laser welding of Ti6Al4V and lead

metal [J]. Journal of Materials Processing Technology, 2012, 212: 1520−1527.

[26] ZHENG Xiu-Lin. Mechanical properties of materials [M]. 2nd ed. Xi'an: Northwestern Polytechnical University Press, 2007. (in Chinese)

[27] ZHANG Qiang, CHEN Jing, WANG Li-lin. Solidification microstructure of laser additive manufactured Ti−6Al−2Zr−2Sn−3Mo−1.5Cr−2Nb titanium alloy [J]. Journal of Materials Science and Technology, 2016, 32: 381−386.

[28] VRANCKEN B, THIJS L, VAN H J. Microstructure and mechanical properties of a novel β titanium metallic composite by selective laser melting [J]. Acta Materialia, 2014, 68: 150−158.

[29] SUN Xiao-min, LIU Dong, TANG Hai-bo. Solid-state phase transformation and microstructure of laser direct manufactured TC17 titanium alloy components [J]. Rare Metal Materials and Engineering, 2013, 42: 724−729. (in Chinese)

激光增材修复 Ti17 钛合金的显微组织与力学性能

赵 庄[1,2]，陈 静[1,2]，张 强[1,2]，谭 华[1,2]，林 鑫[1,2]，黄卫东[1,2]

1. 西北工业大学 凝固技术国家重点实验室，西安 710072；

2. 西北工业大学 金属高性能增材制造与创新设计工业与信息化部重点实验室，西安 710072

摘 要：采用同步送粉激光增材制造技术修复带有小比例表面缺陷的锻造 Ti17 钛合金，系统研究其显微组织、显微硬度及室温拉伸性能。结果表明，和大比例体修复试样相比，小比例表面修复由于缺乏足够的后续热循环，激光沉积区没有α相析出，初始β晶内由典型凝固胞晶组织组成，从而使得激光沉积区显微硬度低于由双态组织构成的锻造基材区。拉伸测试结果表明，在拉伸过程中，激光修复试样存在显著的塑性变形不均匀性，最大应变始终偏聚于激光修复区，且最终以准解理方式断裂于修复区。激光修复试样的抗拉强度略高于锻件试样，而伸长率(11.7%)低于后者。

关键词：激光增材修复；Ti17 钛合金；显微组织；力学性能；变形行为

(Edited by Xiang-qun LI)